

Article

Study on the Impact of Closed Coal Mines on Groundwater in the Panlong River Basin (Shandong Province, China) Based on Sulfur and Oxygen Isotopes

Hao Chen ^{1,2}, Hongnian Chen ^{1,2,3}, Feng Zhang ^{1,2,3}, Zhantao Han ⁴, Huijian Shi ^{5,*}, Jia Meng ^{1,2}, Qiyang Feng ⁶ and Di Chen ⁶

¹ Shandong Provincial Lunan Geology and Exploration Institute (Shandong Provincial Bureau of Geology and Mineral Resources No. 2 Geological Brigade), Jining 272100, China; lnychenhao@163.com (H.C.); 13864171123@126.com (H.C.); lnyzhangfeng@163.com (F.Z.); mdajia@126.com (J.M.)

² Key Laboratory of Karst Geology, Shandong Provincial Bureau of Geology and Mineral Resources, Jining 272100, China

³ Institute of Advanced Studies, China University of Geosciences, Wuhan 430078, China

⁴ Technical Centre for Soil, Agriculture and Rural Ecology and Environment, Ministry of Ecology and Environment, Beijing 100012, China; hanzhantao1977@163.com

⁵ Center for Soil Pollution Control of Shandong, Department of Ecological Environment of Shandong Province, Jinan 250101, China

⁶ School of Environment Science and Spatial Informatics, China University of Mining and Technology, Xuzhou 221116, China; fqycumt@126.com (Q.F.); xinmaichen919@163.com (D.C.)

* Correspondence: 13791090303@163.com

Abstract: To deeply investigate the impact of closed coal mines on groundwater sulfate contamination in the Panlong River basin, Zaozhuang, Shandong Province, China, the hydrochemical characteristics and controlling factors of groundwater were analyzed based on 64 surface water and groundwater samples. The sources of sulfate contamination were identified by sulfur and oxygen isotope analysis. The results indicate that the sulfate content in the pore groundwater exceeds the Standard for Groundwater Quality (China) Category III (250 mg/L), with a maximum content of 666.2 mg/L. Specifically, the exceedance rate of sulfate in pore water near the western boundary of the Taozao coal field is directly related to mine water. The exceedance rate of sulfate in karst groundwater is 28%, peaking at 1131 mg/L, and is mainly distributed outside the western boundary of the Taozao coalfield and near the Dingzhuang water source in the southeast of the coalfield, indicating a significant influence from high-sulfate mine water in the coal-bearing strata. The sulfur and oxygen isotope differences are significant between surface water, mine water, karst water, and pore water. Through Bayesian end-member analysis, it was determined that 40–83% of sulfate in the downstream pore water of the Taozao coal field originated from mine water, while 48–86% of the sulfate in the karst water originated from mine water, which greatly affects the groundwater in the western and southeastern parts of the Taozao coalfield. Therefore, measures should be taken as soon as possible to control the risk of sulfate pollution of neighboring groundwater, especially karst groundwater, by mine water from closed coal mines.

Keywords: groundwater; sulfate; pollution identification; sulfur and oxygen isotopes; closed coal mines



Citation: Chen, H.; Chen, H.; Zhang, F.; Han, Z.; Shi, H.; Meng, J.; Feng, Q.; Chen, D. Study on the Impact of Closed Coal Mines on Groundwater in the Panlong River Basin (Shandong Province, China) Based on Sulfur and Oxygen Isotopes. *Water* **2024**, *16*, 1634. <https://doi.org/10.3390/w16111634>

Academic Editor: Christos S. Akrotos

Received: 9 May 2024

Revised: 3 June 2024

Accepted: 4 June 2024

Published: 6 June 2024



Copyright: © 2024 by the authors. Licensee MDPI, Basel, Switzerland. This article is an open access article distributed under the terms and conditions of the Creative Commons Attribution (CC BY) license (<https://creativecommons.org/licenses/by/4.0/>).

1. Introduction

Hydrochemical composition is a key element in evaluating the quality of surface water and groundwater of a region, as well as its development and utilization. The hydrochemical composition of surface water and groundwater in a region is influenced by multiple factors such as rock weathering, runoff, source conditions, human activities, and climate [1–3].

Meanwhile, based on the chemical parameters of various water bodies and statistical graphical interpretation, the sources and transformation patterns of hydrochemical ions in surface water and groundwater can be obtained [4]. Using the hydrochemical statistical graphical interpretation method, Zhou et al. investigated the main ion characteristics of surface water in the upper reaches of the Shule River basin and the possible controls [5]. Li et al. used a similar approach and analyzed the hydrochemical characteristics of karst groundwater during different hydrological periods. They also explored the natural factors and human factors affecting the major chemical ions [6]. In addition to hydrochemical composition analysis, due to the exchange of substances and energy along with the transformation processes of different water bodies, comprehensive studies of hydrochemical and isotopic compositions of water bodies can also reveal the sources and cyclic process of surface water and groundwater [7,8]. Gu et al. investigated the relationship between surface water and groundwater in the Liujiang Basin using hydrochemistry and environmental isotope analysis [9]. Liu et al. applied hydrochemistry and hydrogen and oxygen stable isotope analysis to reveal that the ion content in different water bodies of the Donggong River Basin is affected by rainfall, temperature, and geological background [10].

Stable isotopes can be employed to identify the sources of water pollution. Sulfur isotopes in nature exhibit a unique isotopic composition that can be attributed to their source [11]. Furthermore, apart from sulfate-reducing bacteria, no significant sulfur isotope fractionation occurs during the biogeochemical sulfur cycle [12]. These characteristics render sulfur isotopes an invaluable tool for tracing the origins of sulfate in water bodies [13,14]. Ma et al. [15] studied the source of sulfate in groundwater in Zaozhuang City (Shandong province, China) using the relationship between $\delta^{34}\text{SSO}_4\text{-SO}_4$, $\delta^{34}\text{SSO}_4\text{-SI}$ (gypsum), and $\delta^{34}\text{SSO}_4\text{-SO}_4^{2-}/\text{Cl}^-$. Based on the distribution characteristics of $\delta^{34}\text{SSO}_4\text{-SO}_4$, $\delta^{34}\text{SSO}_4\text{-SI}$ (gypsum), and $\delta^{34}\text{SSO}_4\text{-SO}_4^{2-}/\text{Cl}^-$, it is believed that sulfate pollution mainly originates from pyrite oxidation, gypsum dissolution and industrial and agricultural wastewater infiltration pollution, and in addition to the primary geological genesis, the infiltration of wastewater discharged by industrial and mining enterprises into the subsurface is also the main cause of sulfate pollution in groundwater. Zhang et al. [16] selected three groundwater potential sulfate source end elements, (A) sulfide oxidation SO_4^{2-} , (B) evaporite dissolution SO_4^{2-} , and (C) atmospheric precipitation SO_4^{2-} , and determined the degree of karst groundwater pollution by mine water using the relationship between $\delta^{34}\text{S}$ (SO_4) and $1/\text{SO}_4^{2-}$ of water samples in the study area combined with the calculation of mixing ratio. Zhao et al. [17] used $\delta^{34}\text{SSO}_4\text{-SO}_4$ correlation to study the SO_4^{2-} source of karst water in the Niangziguan spring area of Shanxi, and determined the source of SO_4^{2-} in different sections according to its distribution characteristics; the SO_4^{2-} in karst water in the northwest and southwest of the Niangziguan spring area mainly originated from the dissolution of gypsum, and the central part of the spring area had a high SO_4^{2-} concentration but a low $\delta^{34}\text{SSO}_4$ values. The authors hypothesized that the SO_4^{2-} contamination may originate from the mine water of the coal system.

The Taozao coalfield, situated in the central-eastern region of Zaozhuang City, Shandong Province, China, is a syncline extending in an east-west direction. It is part of the Carboniferous-Permian coalfield, which is bounded by faults of Beishan on its north side and seam outcrops on its east, west, and south sides. The coalfield extends for a length of 30 km in an east-west direction, with a width of 6 to 7 km in the north-south direction in the western part and 3 to 5 km in the eastern part. It covers an area of 90.10 km². The coalfield has a long history of exploitation, with abundant coal resources. Following the closure of coal mines within the coalfield, there has been a significant rebound in formation water, which has changed the hydrodynamic conditions of the Taozao Basin. This may have an impact on the water quality of the surrounding karst water. The Panlong River is an important surface water body in Zaozhuang City. Therefore, this paper aims to clarify the impact of closed coal mine drainage on the Panlong River and regional groundwater. Firstly, surface water and groundwater samples were collected and tested. Next, the chemical characteristics of groundwater ions were analyzed, and analysis of the sulfur and oxygen

isotopes was applied to identify the pollution sources of groundwater sulfates. The findings of the study could serve as a scientific foundation for further assessment and prevention of groundwater sulfate pollution.

2. Study Area

The study area is situated within a warm and semi-humid continental monsoon climate, characterized by a moderate climate and distinct seasons. The precipitation is concentrated primarily from June to September, accounting for 80.5% of the total annual precipitation. The average precipitation over the period from 1980 to 2021 was 796.89 mm. The sunshine time is around 2380 h, the frost-free period is more than 200 d, and the average annual temperature is 13.9 °C. The study area is part of the Nansi Lake system in the Huai River Basin along the Grand Canal, with a well-developed surface water system. Major rivers include the Panlong River and its major tributaries, which flow from the north to the south, as well as the Dasha River in the Yicheng district. The Panlong River traverses the central and western regions, with its upper reaches divided into two branches: the south branch, which originates from Xingyu-Hengshankou in Xuecheng District, and the north branch, which originates from Baishan in Shizhong District. The drainage area of the north branch is 296 km². As a rain-fed river, it receives surface runoff from the basin and a certain amount of industrial and mining enterprises' production and domestic sewage, which results in severe water pollution during the dry season.

The Taozao Basin exhibits pronounced topographical undulations. It is an irregular elliptical basin extending from east to west, displaying higher elevations in the north, south, and east and lower elevations in the west, with a relatively flat central section. The area comprises Quaternary unconsolidated porous aquifer groups, clastic rocks porous aquifer groups in the overlying strata of coal measure strata, the Carboniferous-Permian rocks fractured aquifer groups, old pits and water-filling roadway aquifer groups in coal seams (aquifer groups of coal measure strata) and karst aquifer groups of Cambrian-Ordovician carbonate rocks (Figure 1b). Among these aquifer groups, the water abundance of water in Quaternary unconsolidated porous aquifer groups is relatively low. The fractures in the overlying strata of the coal measure strata are poorly developed, resulting in a low water inflow per unit. The medium-bedded sandstone within the Carboniferous-Permian rocks fractured aquifer groups has a weak water abundance, and the shale has an extremely poor water abundance. While the shale layers between the coal seam floor and the Ordovician limestone act as relatively impermeable formations. The fractured rock karst aquifers of the Ordovician Majiagou group have undergone strong karst development, forming cool springs and sources of drinking water on the surface. In the Cambrian carbonate rock fractured karst aquifer groups, the karst features are well developed and the aquifers have abundant water, forming Shili Spring and Dingzhuang–Dongwangzhuang headwaters. Following the closure of mines, mine water infiltrates into the deep confined water through skylights, abandoned fractured wells, and faults, resulting in the pollution of the karst underground water.

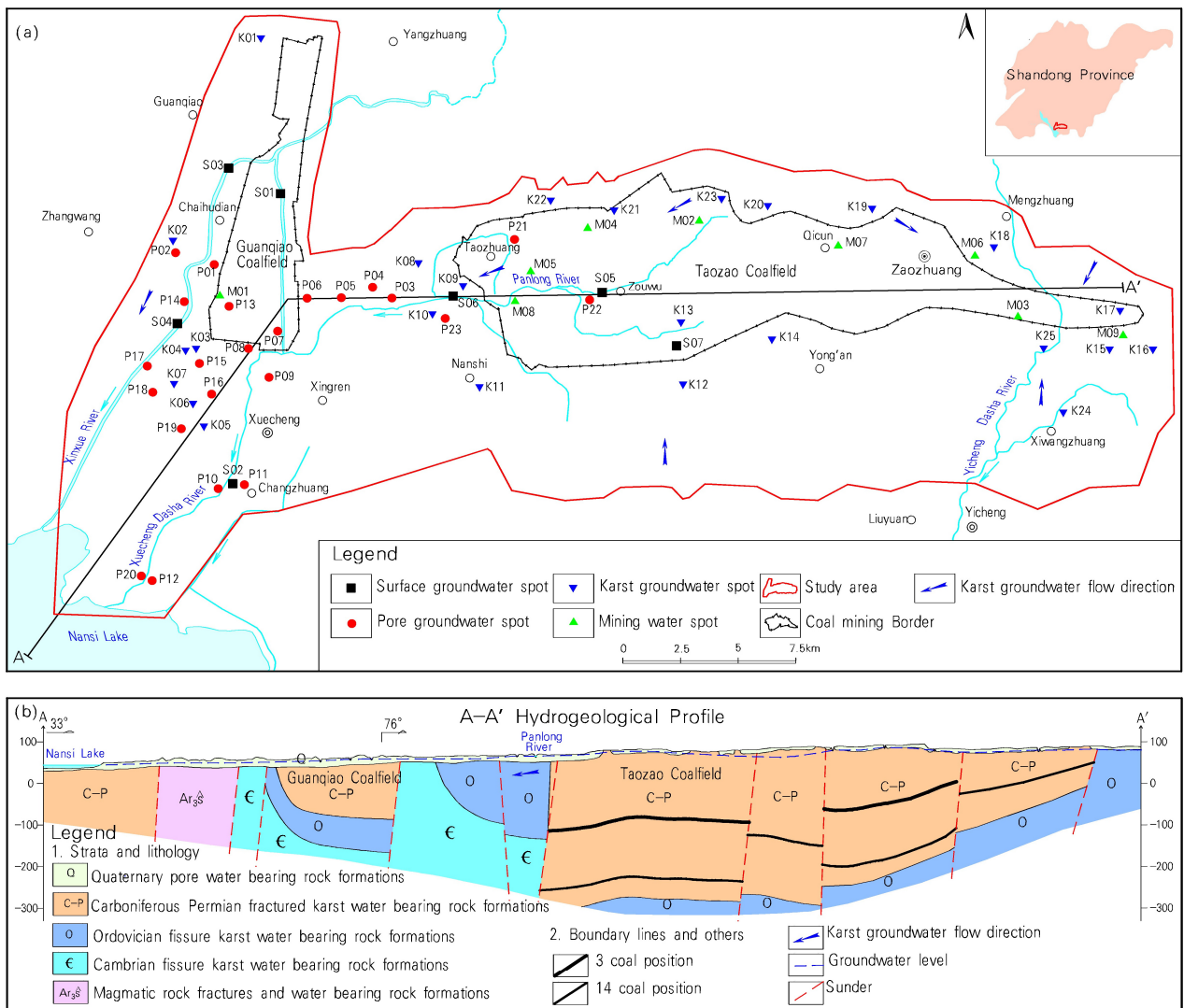


Figure 1. Distribution of sampling points and formations in the study area. (a) Distribution of sampling points (b) Hydrogeological profile of study area).

3. Sampling and Analysis Methods

3.1. Sample Collections

After a comprehensive examination of the characteristics of groundwater flow and the impact range of abandoned mines, a total of 64 sampling points were established in this survey (Figure 1a), comprising 7 surface water sampling points, 23 points of Quaternary pore water (referred to as pore water), 9 points of water in coal measure strata fissures (referred to as mine water), and 25 points of karst groundwater (referred to as karst water). Prior to sample collection, the wells were washed using portable water quality test kits, which were used to perform water quality tests every five minutes until at least three consecutive measurements of at least three testing indexes reached stable standards for groundwater sample collection. If these standards were not achieved after four hours of washing, Bailer’s method was applied for sampling. Once the water quality stabilized, sample collection began and was completed within two hours. The samples were stored at 4 °C and sent to the laboratory within 24 h for analysis.

3.2. Physical-Chemical Testing

A handheld GPS locator was employed to ascertain the coordinates of each sampling point. On-site pH and temperature measurements were conducted using a portable water

quality testing kit (Hach DS5, Loveland, CO, USA) and total dissolved solids (TDS) were quantified using a portable conductivity meter (SX-650). Anions, namely chloride (Cl^-), sulfate (SO_4^{2-}), nitrate (NO_3^-), and fluoride (F^-), were analyzed using a Thermo Scientific™ Dionex™ Aquion™ Ion Chromatography (IC) instrument (Waltham, MA, USA). The concentration of HCO_3^- was determined by titration with methyl orange as the indicator. K^+ and Na^+ were quantified using an atomic absorption spectrophotometer (GFA-6880 by Shimadzu Corporation, Kyoto, Japan). Ca^{2+} and Mg^{2+} were determined by titration with ethylenediaminetetraacetic acid (EDTA). Total nitrogen (TN) was quantified by alkaline potassium persulfate digestion UV spectrophotometry in accordance with the current national standard. The total phosphorus (TP) concentration was quantified by the ammonium molybdate spectrophotometric method. The total iron (Fe) and manganese (Mn) concentrations were determined by inductively coupled plasma spectroscopy (ICP). All samples were analyzed by the Water and Soil Testing Center of the Shandong Provincial Lunan Geology and Exploration Institute. The national standard [18] was used to conduct quality assurance and quality control (QA/QC) of the ion determinations. During the analysis, three replicate water samples were used to assess the precision of the analysis. The analytical precision of the ion charge balance was within 5% for all water samples.

Each sample for sulfate and oxygen isotope was collected at 1.5 L on the site and filtered through cellulose acetate membranes within 24 h. Thereafter, 1 mL of high-purity concentrated hydrochloric acid was added, mixed well, and allowed to stand for 0.5 h. Next, 10 mL of saturated BaCl_2 solution was added to the sample, which was then left to stand overnight. The precipitate of BaSO_4 was filtered by a PES membrane with a pore size of 0.22 μm (or a cellulose acetate membrane with a pore size of 0.45 μm) in the laboratory and then dried at 850 °C for 2 h. Subsequently, purification of BaSO_4 samples was carried out. The dried BaSO_4 solids were transferred and dissolved in a DTPA solution. Once all the precipitate had dissolved, high-purity concentrated hydrochloric acid was added to remove the carbonate. Then, a saturated barium chloride solution was added to re-precipitate the sulfate ions. After washing with ultrapure water to remove BaCl_2 and DTPA, the samples were dried at 60 °C for more than 24 h [19]. After purification, the dried BaSO_4 precipitate underwent testing for sulfur and oxygen isotopes in sulfate at Nanjing University. Sulfur and oxygen isotopes were tested using the EA Isolink-Conflo IV-Delta V plus and EA-HT Isolink-Conflo IV-Delta V plus instruments, respectively. The international standard (NBS127, $\delta^{18}\text{O}_{\text{VMSOW}} = 8.6\text{‰}$; $\delta^{34}\text{S}_{\text{VCDT}} = 20.3\text{‰}$) was chosen to calibrate the samples to be tested, all with an analytical accuracy of $\pm 0.3\text{‰}$.

3.3. Analysis of Stable Isotopes

A Bayesian isotope mixing model was employed to determine the proportions of sulfates in water [20]. The fundamental premise is elucidated by the following formula:

$$X_{ij} = \varepsilon_{ij} + \sum_{k=1}^k P_k (S_{jk} + C_{jk}) \quad (1)$$

$$S_{jk} \sim N(\mu_{jk}, \omega_{jk}^2) \quad (2)$$

$$C_{jk} \sim N(\lambda_{jk}, \tau_{jk}^2) \quad (3)$$

$$\varepsilon_{ij} \sim N(0, \sigma_j^2) \quad (4)$$

In this context, k represents the number of potential sources; i represents the number of samples of the mixture, and $i = 1, 2, 3, \dots, N$; j represents the type of stable isotope, and $j = 1, 2, 3, \dots, J$; X_{ij} represents the composition of isotope j in the i th mixture; P_k represents the mixing ratios of each potential source, which are the final result calculated by the model. For multi-element isotopes, the model requires the input of the j th isotopic composition range S_{jk} in the k th potential source, represented by mean μ_{jk} and standard deviation ω_{jk} . For defining the isotope fractionation during the process from source to

mixture, the fractionation factor C_{jk} of the j th isotope in the k th potential source is input to the model, represented by mean λ_{jk} and variance τ_{jk} . In the absence of isotope fractionation, the fractionation factor C_{jk} may be disregarded. ϵ_{ij} refers to additional unquantifiable differences between mixture i , typically represented by a mean of 0 and a variance of σ_j .

4. Results and Discussions

4.1. Hydrochemical Characteristics of Water Samples

The statistical analysis of conventional hydrochemical parameters for the surface water and groundwater samples is presented in Table 1. The range of total dissolved solids (TDS) in the surface water samples is 385.00 to 1382.00 mg/L, with an average of 1049.80 mg/L. The most abundant cations are Ca^{2+} and Na^+ , with mean mass concentrations of 183.10 mg/L and 89.00 mg/L, respectively. The main anions are SO_4^{2-} and HCO_3^- , with mean mass concentrations of 535.88 mg/L and 209.08 mg/L respectively. TDS in the pore groundwater samples ranges from 389.00 to 2156.00 mg/L, with an average of 985.78 mg/L, predominantly freshwater. The order of cation mass concentrations is as follows $Ca^{2+} > Na^+ > Mg^{2+} > K^+$, with averages of 233.81 mg/L, 49.16 mg/L, 32.87 mg/L, and 1.12 mg/L, respectively. The order of anion mass concentrations is as follows: $HCO_3^- > SO_4^{2-} > Cl^- > NO_3^-$, with mean values of 373.75 mg/L, 272.01 mg/L, 125.15 mg/L, and 18.48 mg/L, respectively, showing significant differences. NO_3^- concentrations in more than 50 percent of the wells exceeded the Standard for Groundwater Quality (China) [21] Category III, followed by SO_4^{2-} , exceeding 39%. The range of TDS is 670.00~3620.00 mg/L in mine water, with an average of 2064.3 mg/L, and brackish water accounts for 34.7%. The order of cation mass concentrations is as follows: $Ca^{2+} > Na^+ > Mg^{2+} > K^+$, with average of 279.08 mg/L, 128.50 mg/L, 51.84 mg/L, and 7.61 mg/L, respectively. The order of anion mass concentrations is as follows: $SO_4^{2-} > HCO_3^- > Cl^- > NO_3^-$, with mean values of 657.16 mg/L, 424.08 mg/L, 75.00 mg/L, and 14.99 mg/L, respectively, showing great differences. The anion with the highest rate of exceedance of the standard is SO_4^{2-} , with an exceedance of 78%, followed by NO_3^- , with an exceedance of 44%.

Table 1. Statistical results of major hydrochemical indicators for different water bodies.

Indicators	Surface Water (n = 7)					Pore Water (n = 23)					Mine Water (n = 9)					Karst Water (n = 25)				
	Min.	Max.	Avg.	SD	CV	Min.	Max.	Avg.	SD	CV	Min.	Max.	Avg.	SD	CV	Min.	Max.	Avg.	SD	CV
TDS (mg/L)	385.00	1382.00	1049.80	398.80	0.38	389.00	2156.00	985.78	329.82	0.33	670.00	3620.00	2046.3	831.15	0.56	459.00	2139.00	868.96	347.75	0.40
TP	0.01	0.13	0.04	0.05	1.06	0.007	0.064	0.028	0.01	0.53	0.011	0.103	0.032	0.03	0.83	0.007	0.126	0.027	0.02	0.81
TN	0.20	4.20	1.37	1.27	0.93	0.31	48.44	18.91	14.23	0.75	0.296	37.763	14.609	14.93	1.02	0.67	45.68	13.97	9.57	0.68
K^+ (mg/L)	3.9	8.3	5.4	1.42	0.26	0.33	2.21	1.12	0.54	0.48	0.91	33.41	7.61	9.57	1.26	0.73	13.81	1.98	2.52	1.27
Na^+ (mg/L)	27.2	139.4	89.0	36.94	0.415	16.16	134.65	49.15	34.03	0.69	28.958	618.412	128.499	175.77	1.37	9.40	221.51	47.98	50.60	1.05
Ca^{2+} (mg/L)	56.2	278.3	183.1	80.83	0.44	97.97	461.82	233.81	71.32	0.31	158.44	399.025	279.082	81.02	0.29	125.74	370.72	192.69	61.47	0.32
Mg^{2+} (mg/L)	13.4	56.8	41.4	16.93	0.41	14.24	89.32	32.87	16.36	0.50	22.78	135.358	51.839	34.90	0.67	11.43	64.20	32.49	13.70	0.42
Cl^- (mg/L)	28.13	131.34	80.76	30.20	0.37	34.53	539.55	125.15	104.91	0.84	42.087	125.168	75.003	26.58	0.35	8.48	133.42	66.05	32.17	0.49
SO_4^{2-} (mg/L)	122.84	901.62	535.88	278.77	0.52	40.97	665.72	272.01	155.14	0.57	221.125	2049.01	657.16	566.30	0.86	106.09	1131.35	296.52	230.37	0.78
HCO_3^{2-} (mg/L)	117.22	306.20	209.08	71.78	0.34	270.32	527.48	373.75	65.75	0.18	258.355	729.61	424.08	126.77	0.30	220.08	497.57	332.18	56.87	0.17
NO_3^- (mg/L)	0.05	2.40	0.93	0.83	0.89	0.19	45.67	18.48	12.73	0.69	0.248	37.72	14.99	14.48	0.97	0.50	42.09	13.13	9.18	0.70
F^- (mg/L)	0.09	0.87	0.53	0.30	0.57	0.07	0.71	0.27	0.18	0.67	0.057	0.351	0.183	0.09	0.47	0.035	0.27	0.14	0.06	0.41
Fe (μ g/L)	23.86	121.21	55.38	32.26	0.58	20.32	1174.50	117.09	229.96	1.96	44.43	22032.00	2731	6070.82	1.86	19.313	2268.56	307.41	575.57	1.87
Mn (μ g/L)	4.67	913.17	342.21	335.09	0.98	1.69	1897.55	238.77	483.85	2.03	0.70	5478	1898	1170.05	1.59	0.651	467.37	38.97	94.71	2.43

The iron content in the mine water samples ranges from 0.044 to 22.032 mg/L, with an average of 2.731 mg/L, while manganese content ranges from 0.0007 to 5.478 mg/L, with

an average of 1.898 mg/L. TDS in the karst groundwater samples ranges from 459.00 to 2139.00 mg/L, with an average of 868.96 mg/L. Brackish water accounts for 24%. The order of cation mass concentrations is as follows: $\text{Ca}^{2+} > \text{Na}^+ > \text{Mg}^{2+} > \text{K}^+$, with the average of 192.70 mg/L, 47.99 mg/L, 32.49 mg/L, and 1.99 mg/L, respectively. The order of anion mass concentrations is as follows $\text{HCO}_3^- > \text{SO}_4^{2-} > \text{Cl}^- > \text{NO}_3^-$ (as N), with the main values of 332.18 mg/L, 296.53 mg/L, 66.06 mg/L, and 13.13 mg/L, respectively, showing significant differences. The anion with the highest exceedance rate is SO_4^{2-} with 24%, followed by NO_3^- , with 16%.

The analysis shows that the dominant cations in groundwater are Ca^{2+} and Na^+ , while the dominant anions in pore and karst groundwater are HCO_3^- , followed by SO_4^{2-} . In mine water, the dominant anion is SO_4^{2-} , followed by HCO_3^- . From the coefficient of variation, the coefficients of variation of total phosphorus in surface water, total nitrogen, K^+ and Na^+ in mine water, and K^+ and Na^+ in karst water were slightly higher than 1. The coefficients of variation of total iron and manganese were larger in pore water, mine water, and karst water (1.86–1.96, 1.59–2.43), and the coefficients of variation of the rest of the indexes were all less than 1, which indicated that the spatial distribution of total iron and manganese was extremely unequal; in addition to being affected by mine mining activities, these indexes are also affected by stratigraphic factors and redox environment, etc.

4.2. Hydrochemical Types Analysis

A Piper trilinear diagram is a commonly used tool for presenting water chemistry data. Its purpose is to directly represent the relative abundance and distribution characteristics of major ions in water chemistry, thereby assisting in the identification of end-members of hydrochemical formation and evolution [22]. As illustrated in Figure 2, the distribution of hydrochemical types is relatively concentrated, with cations predominantly distributed near the Ca^{2+} and Mg^{2+} ends, while anions are mainly distributed near the HCO_3^- and SO_4^{2-} ends. In particular, pore groundwater is primarily of the $\text{HCO}_3\text{-SO}_4\text{-Ca}$ and $\text{HCO}_3\text{-Ca}$ types, accounting for 56.5% and 13.0%, respectively. Karst groundwater and mine water are mainly of the $\text{HCO}_3\text{-SO}_4\text{-Ca}$ types, accounting for 80.0% and 77.7%, respectively. This indicates that each water body is mainly influenced by carbonate rock weathering and dissolution, in the form of sulfide mineral oxidation and sulfate mineral dissolution.

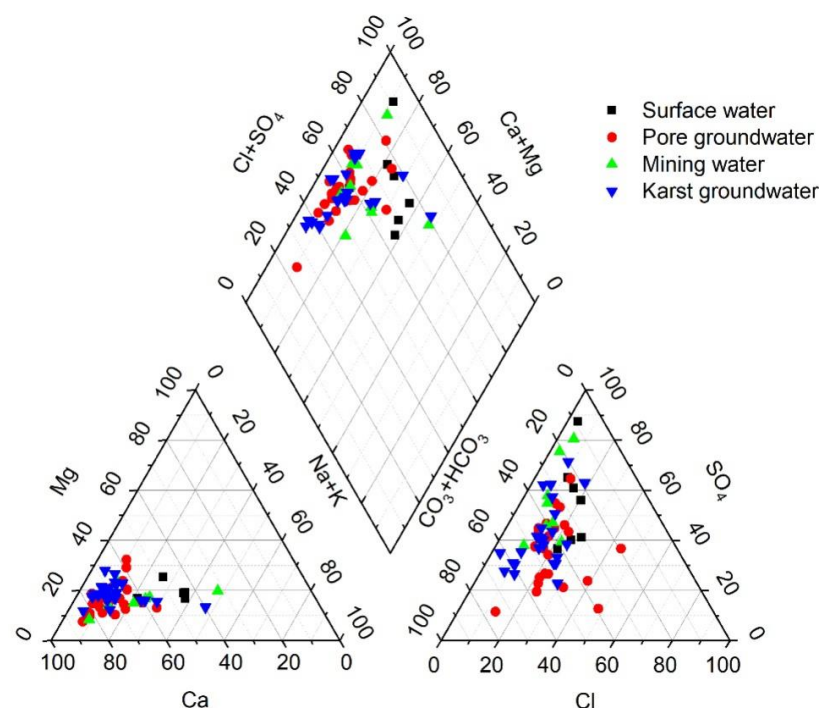


Figure 2. Piper trilinear diagrams.

4.3. Analysis of Water–Rock Interaction of Water Samples

The primary sources of Na^+ and K^+ in natural water bodies are the weathering of silicate minerals and evaporite rocks. Cl^- remains relatively stable in groundwater and is mainly derived from the weathering and dissolution of evaporite rocks. When Na^+ , K^+ , and Cl^- in groundwater are derived from the weathering and dissolution of rock salts in the aquifer, the value of $\gamma(\text{Na}^+ + \text{K}^+)/\text{Cl}^-$ should be equal to 1. Figure 3a illustrates the distribution of sampling points across the study area, which is generally scattered. In pore groundwater, the ratio of $(\text{Na}^+ + \text{K}^+)$ to Cl^- is less than 1 for most ions, indicating that except for the dissolution of rock salts, Na^+ and K^+ can more easily be absorbed by mineral surfaces and Cl^- may be influenced by anthropogenic pollution. In contrast, for some karst groundwater, the ratio of $(\text{Na}^+ + \text{K}^+)$ to Cl^- is greater than 1, indicating that the Na^+ , K^+ , and Cl^- mainly originate from the weathering and dissolution of evaporite rocks. Nevertheless, $\gamma(\text{Na}^+ + \text{K}^+)/\text{Cl}^-$ is less than 1 in certain locations, suggesting the potential influence of other sources. For mine water and surface water, $\gamma(\text{Na}^+ + \text{K}^+)/\text{Cl}^-$ is more than 1, indicating that Na^+ and K^+ in groundwater are not balanced by Cl^- . This could be attributed to ion exchange among Na^+ , Ca^{2+} , and Mg^{2+} [23], or potential influences from other sources of Na^+ , such as anthropogenic inputs, etc.

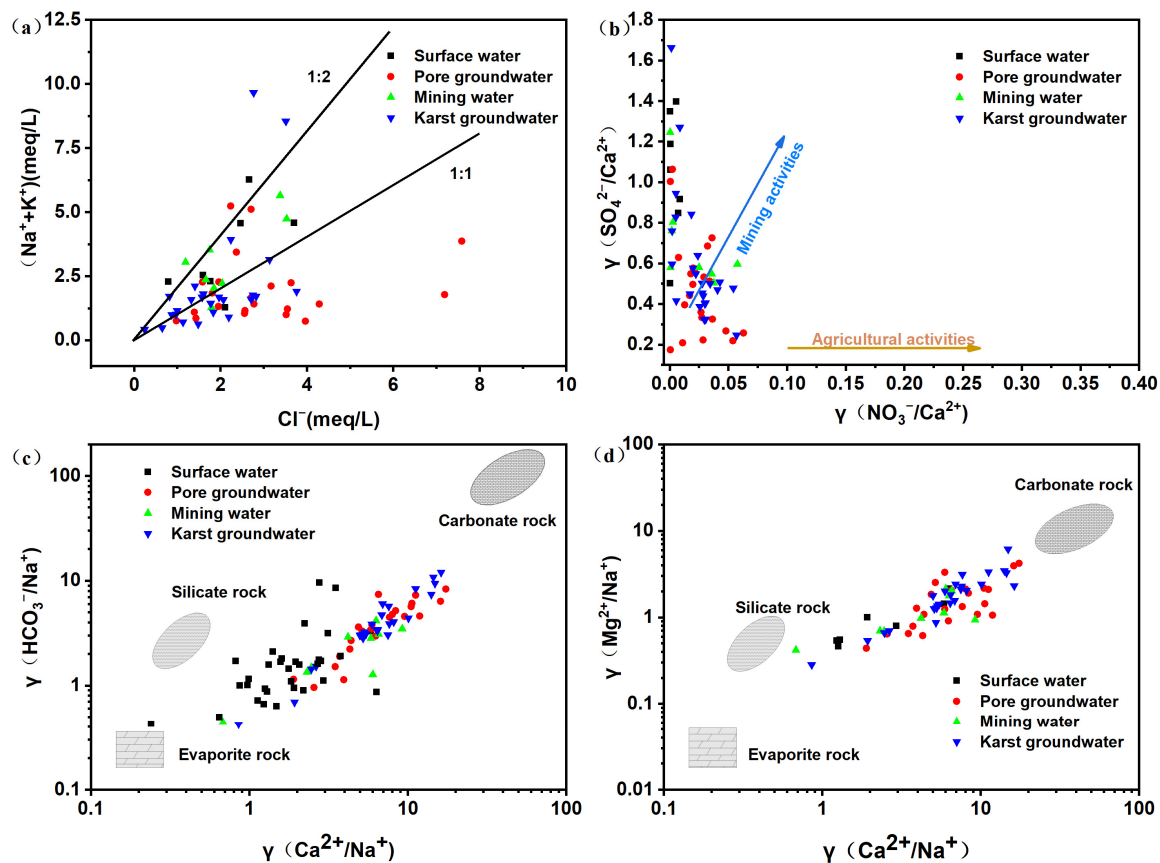


Figure 3. Ion-ratio relationship diagrams in the study area. (a) the relationship of $\text{Na}^+ + \text{K}^+$ and Cl^- (b) the relationship of $\gamma(\text{SO}_4^{2-}/\text{Ca}^{2+})$ and $\gamma(\text{NO}_3^-/\text{Ca}^{2+})$ (c) the relationship of $\gamma(\text{HCO}_3^-/\text{Na}^+)$ and $\gamma(\text{Ca}^{2+}/\text{Na}^+)$ (d) the relationship of $\gamma(\text{Mg}^{2+}/\text{Na}^+)$ and $\gamma(\text{Ca}^{2+}/\text{Na}^+)$.

In general, agricultural activities exhibit relatively high $\text{NO}_3^-/\text{Ca}^{2+}$ values and low $\text{SO}_4^{2-}/\text{Ca}^{2+}$ values, whereas mining activities exhibit the opposite trend [24]. Figure 3b illustrates this trend, with surface water and mine water showing low $\text{NO}_3^-/\text{Ca}^{2+}$ values and high $\text{SO}_4^{2-}/\text{Ca}^{2+}$ values in the study area. The majority of points are distributed in the upper-left area of the diagram. This indicates that surface water and mine water are significantly impacted by mining activities. For pore water and karst water, some points

exhibit similar distributions to surface water and mine water, being also located in the upper-left area of the diagram. This suggests that pore water and karst water are also influenced by mining activities in the study area. Based on the hydrochemical characteristics of single lithological small watersheds, Gaillardet et al. [25] summarized the hydrochemical characteristics of end-members of silicate rocks, evaporite rocks, and carbonate rocks. The influence of rock weathering on water solutes can be distinguished through relationships between $\text{Ca}^{2+}/\text{Na}^+$ and $\text{HCO}_3^-/\text{Na}^+$ and $\text{Ca}^{2+}/\text{Na}^+$ and $\text{Mg}^{2+}/\text{Na}^+$. Figure 3c,d demonstrate that the sampling points are concentrated between the end-members of evaporite rocks and carbonate rocks. This indicates that the hydrochemical ions in this area are primarily derived from the weathering and dissolution of evaporite and carbonate rocks.

4.4. Sulfur and Oxygen Isotope Characteristics

The use of sulfur and oxygen isotope analysis allows for the effective identification of the sources of sulfate ions. The sulfur isotopic composition of sulfate ions, as indicated by $\delta^{34}\text{S}_{\text{SO}_4}$, can provide insights into the sources and chemical transformation processes. In contrast, the oxygen isotopic composition of sulfate ions, as indicated by $\delta^{18}\text{O}_{\text{SO}_4}$, can provide insights into the redox environment. Table 2 indicates that the average $\delta^{34}\text{S}_{\text{SO}_4}$ of pore groundwater, mine water, and karst water are 3.16‰, 0.23‰, and 2.44‰, respectively, while the average $\delta^{18}\text{O}_{\text{SO}_4}$ are +3.90‰, 2.96‰, and 3.88‰, respectively. Except for mine water wells M04, M05, and M07, which have relatively shallow depths (wells less than 10 m deep) and low water table burial depths, resulting in larger $\delta^{18}\text{O}_{\text{SO}_4}$, all other mine water wells have relatively lower $\delta^{34}\text{S}_{\text{SO}_4}$ and $\delta^{18}\text{O}_{\text{SO}_4}$. The potential sources of SO_4^{2-} include atmospheric precipitation, rock weathering (gypsum dissolution and pyrite oxidation), and anthropogenic factors [24], among others. Different sources of SO_4^{2-} have distinct $\delta^{34}\text{S}_{\text{SO}_4}$ values. Gypsum in marine sediments typically exhibits higher $\delta^{34}\text{S}_{\text{SO}_4}$ values, as exemplified by the Handan Middle Ordovician gypsum, with $\delta^{34}\text{S}_{\text{SO}_4}$ values ranging from 20‰ to 24‰ [26]. In contrast, pyrite in sedimentary rocks typically exhibits lower $\delta^{34}\text{S}_{\text{SO}_4}$ values. The values range from 3.4‰ to 10.2‰ in coal seams in different regions of China [27], while those in magmatic rocks range from −5‰ to +5‰ [26,28]. There is no significant isotopic fractionation of sulfur during the oxidation of pyrite, so the $\delta^{34}\text{S}_{\text{SO}_4}$ values of SO_4^{2-} formed from oxidation are similar to those of pyrite. Some studies indicate that the $\delta^{34}\text{S}_{\text{SO}_4}$ values of pyrite oxidation products range from −15‰ to 4‰ [29]. The minimum $\delta^{34}\text{S}_{\text{SO}_4}$ and $\delta^{18}\text{O}_{\text{SO}_4}$ values of the samples are negative in the study area, indicating that some of the SO_4^{2-} may originate from the oxidation of sulfide minerals.

Table 2. Statistical results of $\delta^{34}\text{S}_{\text{SO}_4}$ and $\delta^{18}\text{O}_{\text{SO}_4}$ in different water bodies.

Water Bodies		Pore Water	Mine Water	Karst Water
$\delta^{34}\text{S}_{\text{SO}_4}$	Max.	8.0‰	6.4‰	7.8‰
	Min.	−2.5‰	−4.7‰	−3.4‰
	Avg.	3.16‰	0.23‰	2.44‰
	SD	3.36	2.70	2.45
$\delta^{18}\text{O}_{\text{SO}_4}$	Max.	7.9‰	7.4‰	8.8‰
	Min.	−0.2‰	−0.3‰	−4.6‰
	Avg.	3.90‰	2.96‰	3.88‰
	SD	2.79	2.96	2.61

Figure 4a,b illustrate the relationships between $\delta^{34}\text{S}-\text{SO}_4$ and $\delta^{18}\text{O}-\text{SO}_4$ and $\delta^{18}\text{S}-\text{SO}_4$ and SO_4^{2-} in various water bodies within the study area. It is evident that the values of the majority of sample points fall within the range of sulfide mineral oxidation, suggesting that nearby coal mining activities have a significant impact on the sulfate concentration in the regional water bodies. Furthermore, the values of $\delta^{34}\text{S}-\text{SO}_4$ of mine water are lower than those of the other two types of groundwater, indicating a greater influence of mineral

oxidation on coal mine water. Based on the relationships between $\delta^{18}\text{O}\text{-SO}_4$ and SO_4^{2-} , the majority of mine water and some pore water and karst water samples are located in the lower-right area, indicating a significant influence of sulfide mineral oxidation. Some pore water and karst water samples are situated in the upper-right area of gypsum dissolution, indicating that the sulfate concentration in the groundwater is generally higher due to the combined effects of several factors. Moreover, it has been found that the isotopes undergo variations before and after rainfall even at the same sampling point, with an overall increase in atmospheric precipitation after rainfall, and a trend of increasing sulfur and oxygen isotopes.

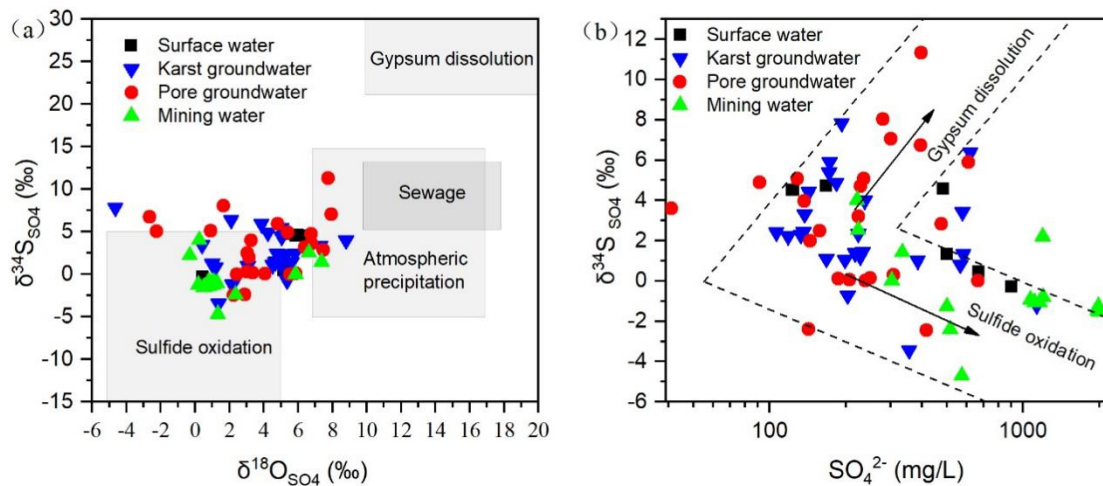


Figure 4. Distribution characteristics of sulfur and oxygen isotopes in water samples in the study area (The gray areas indicate values quoted from Refs. [26–29]). (a) the relationship of $\delta^{34}\text{S}\text{-SO}_4$ and $\delta^{18}\text{O}\text{-SO}_4$ (b) the relationship of $\delta^{34}\text{S}\text{-SO}_4$ and SO_4^{2-} .

4.5. Source Identification of Sulfate

The previous analysis indicates that sulfate in surface water and groundwater in the study area primarily originates from sulfide oxidation, atmospheric precipitation, gypsum dissolution, and sewage discharge. The end-member values for sulfate sulfur and oxygen isotopes in atmospheric precipitation were derived from testing in North China, with $\delta^{34}\text{S}_{\text{SO}_4} = +3\text{‰}$ and $\delta^{18}\text{O}_{\text{SO}_4} = +8\text{‰}$ [30,31]. The end-member values of the $\delta^{34}\text{S}_{\text{SO}_4}$ and $\delta^{18}\text{O}_{\text{SO}_4}$ in sulfide minerals were also calculated using the aforementioned average values, resulting in the following current test values for mine water, $\delta^{34}\text{S}_{\text{SO}_4} = -5\text{‰}$ and $\delta^{18}\text{O}_{\text{SO}_4} = -0.5\text{‰}$ [32,33]. For gypsum in carbonate-evaporite rock, $\delta^{34}\text{S}_{\text{SO}_4}$ is approximately $+25\text{‰}$, while $\delta^{18}\text{O}_{\text{SO}_4}$ typically ranges from $+15\text{‰}$ to $+20\text{‰}$. The $\delta^{34}\text{S}_{\text{SO}_4}$ value was found to be $+25\text{‰}$, while the $\delta^{18}\text{O}_{\text{SO}_4}$ value was 18‰ [34]. Previous studies have indicated that for sewage discharge, the $\delta^{34}\text{S}_{\text{SO}_4}$ value is 8‰ , while the $\delta^{18}\text{O}_{\text{SO}_4}$ value is 15‰ [35]. A Bayesian stable isotope mixing model based on R programming language was employed to calculate the mixing ratios of different sources (<https://cran.r-project.org/web/packages/simmr/vignettes/simmr.html> accessed on 20 January 2024). This model represents an enhanced version of the stable isotope mixing model installation package [36]. Consequently, the mixing ratios of sulfate sources could be calculated within the study area.

Figure 5a,b illustrate the distributions and sources of karst water and pore water in the study area. The distribution contour of sulfate indicates that the concentration of sulfate in the groundwater is increasing in and surrounding the Taozao coalfield, exceeding the groundwater quality standard of 250 mg/L. In particular, sulfate concentrations at some points in the central part of the coalfield exceed 350 mg/L. The analysis of sulfate sources indicates that the average contribution percentages from sulfide minerals, gypsum dissolution, atmospheric precipitation, and sewage sources in karst water are 64.35%, 16.00%, 12.62%, and 7.04%, respectively. This suggests that sulfate in karst water is primarily

derived from the oxidation of sulfide minerals, with some locations exhibiting sulfide mineral contributions as high as 86%. The average contribution percentages from sulfide minerals, gypsum dissolution, atmospheric precipitation, and sewage sources in pore water are 65.13%, 18.30%, 8.55%, and 8.00%, respectively. This indicates that sulfate in pore water also primarily originates from the oxidation of sulfide minerals, with some locations showing sulfide mineral contributions as high as 83%. From the distribution of sampling points, it can be observed that in the vicinity of the western boundary of the Taozao coalfield, the ratio of sulfate in Quaternary pore water originating from the oxidation of sulfide minerals is relatively high, while the ratios in pore water are low in most areas. The values of the other three sources of sulfate pollution are generally similar, indicating that these sources of pollution also contribute to varying degrees of contamination in different water bodies.

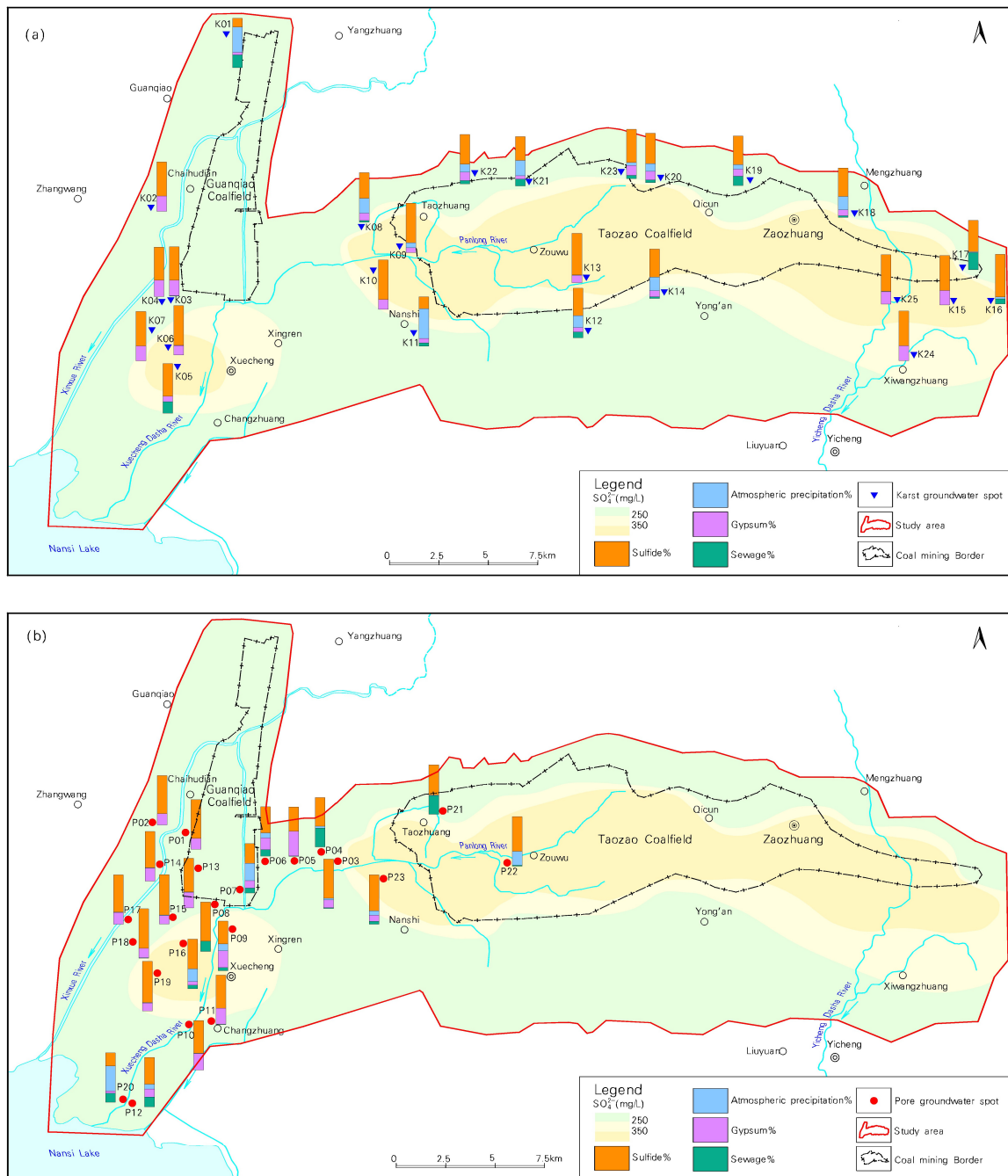


Figure 5. Distributions and sources of sulfate in karst water and pore water. (a) Karst water (b) Pore water.

5. Conclusions

The study area is the Panlong River Basin in Zaozhuang City, Shandong Province, China. The status of sulfate pollution and its sources are analyzed based on chemical and sulfur–oxygen isotope data. The results indicate that the sulfate in Quaternary groundwater exceeds the regulatory limits by 39%, reaching a peak of 666.2 mg/L. Specifically, the pore water near the western boundary of the Taozao coalfield is directly related to mine water recharge. In the downstream area of the Panlong River, Changcun Town, the sulfate exceedance is associated with emissions from paper mills, domestic sewage effluents, and closed coal preparation plants. The sulfate in karst groundwater exceeds regulatory limits by 28%, peaking at 1131 mg/L. It is distributed mainly outside the western boundary of the coalfield and near the Dingzhuang water source in the southeastern part of the coalfield. Its concentration is significantly influenced by mine water with high sulfate levels in coal-bearing strata. Isotope testing results show significant differences in sulfur–oxygen isotopes among surface water, mine water, karst water, and pore water. Bayesian end-member analysis was employed to ascertain the proportions of various sulfate sources. The results indicated that 40–83% of the sulfate in pore water downstream of the Taozao coalfield originated from coal seam water, while 48–86% in karst water was derived from coal seam water, exerting a notable influence on groundwater in the vicinity of the western boundary and southeastern part of the Dingzhuang area within the Taozao coalfield.

Author Contributions: Conceptualization, H.C. (Hongnian Chen), H.S. and Q.F.; Methodology, Q.F.; Software, H.C. (Hongnian Chen); Validation, F.Z.; Formal analysis, F.Z.; Investigation, F.Z. and D.C.; Resources, D.C.; Data curation, Z.H. and J.M.; Writing—original draft, H.C. (Hao Chen) and Z.H.; Writing—review & editing, H.C. (Hao Chen); Supervision, H.C. (Hao Chen); Project administration, H.C. (Hao Chen) and H.S.; Funding acquisition, H.S. All authors have read and agreed to the published version of the manuscript.

Funding: This research was supported by Project: The Investigation and Evaluation Project of Groundwater Environment in Nansi Lake Basin (Grant No. SDGP370000000202202001051).

Data Availability Statement: The original contributions presented in the study are included in the article, further inquiries can be directed to the corresponding author.

Conflicts of Interest: The authors declare no conflict of interest.

References

1. Smith, D.N.; Ortega-Camacho, D.; Acosta-González, G.; Leal-Bautista, R.M.; Fox, W.E.; Cejudo, E. A multi-approach assessment of land use effects on groundwater quality in a karstic aquifer. *Heliyon* **2020**, *6*, e3970. [[CrossRef](#)] [[PubMed](#)]
2. Sheibani, S.; Ataie-Ashtiani, B.; Safaie, A.; Simmons, C.T. Influence of lakebed sediment deposit on the interaction of hypersaline lake and groundwater: A simplified case of lake Urmia, Iran. *J. Hydrol.* **2020**, *588*, 125110. [[CrossRef](#)]
3. Barbieri, M.; Barberio, M.D.; Banzato, F.; Billi, A.; Boschetti, T.; Franchini, S.; Gori, F.; Petitta, M. Climate change and its effect on groundwater quality. *Environ. Geochem. Health* **2023**, *45*, 1133–1144. [[CrossRef](#)] [[PubMed](#)]
4. Junyi, H.; Shi, Y.; Zhang, Q.; Li, L. Hydrochemical characteristics and estimation of the dissolved inorganic carbon flux in the Donghe River Basin of western Hunan. *Hydrogeol. Eng. Geol.* **2019**, *46*, 64–72.
5. Zhou, J.; Ding, Y.; Zeng, G.; Wu, J.; Qin, J. Major Ion Chemistry of Surface Water in the Upper Reach of Shule River Basin and the Possible Controls. *Environ. Sci.* **2014**, *35*, 3315–3324.
6. Li, J.; Zou, S.-Z.; Zhao, Y.; Zhao, R.-K.; Dang, Z.-W.; Pan, M.-Q.; Zhu, D.-N.; Zhou, C.-S. Major Ionic Characteristics and Factors of Karst Groundwater at Huixian Karst Wetland, China. *Environ. Sci.* **2021**, *42*, 1750–1760.
7. Sappa, G.; Vitale, S.; Ferranti, F. Identifying Karst Aquifer Recharge Areas using Environmental Isotopes: A Case Study in Central Italy. *Geosciences* **2018**, *8*, 351. [[CrossRef](#)]
8. Wannous, M.; Theilen-Willige, B.; Troeger, U.; Falk, M.; Siebert, C.; Bauer, F. Hydrochemistry and environmental isotopes of spring water and their relation to structure and lithology identified with remote sensing methods in Wadi Araba, Egypt. *Hydrogeol. J.* **2021**, *29*, 2245–2266. [[CrossRef](#)]
9. Gu, H.; Chi, B.; Wang, H.; Zhang, Y.; Wang, M. Relationship between surface water and groundwater in the Liujiang Basin—Hydrochemical constrains. *Adv. Earth Sci.* **2017**, *32*, 789–799.
10. Bing, L.; He, W.; Jiang, H.; Jia, Y.; Yang, Y.; Gu, H.; Huan, H. Transformation relationship of different water body in Donggong River based on hydrochemistry and hydrogen-oxygen isotopes. *Res. Environ. Sci.* **2020**, *33*, 1979–1990.

11. Nguyen, B.C.; Putaud, J.P. Stable isotopes: Natural and anthropogenic sulphur in the environment. *Atmos. Res.* **1993**, *29*, 275. [[CrossRef](#)]
12. Tuttle, M.; Breit, G.N.; Cozzarelli, I.M. Processes affecting $\delta^{34}\text{S}$ and $\delta^{18}\text{O}$ values of dissolved sulfate in alluvium along the Canadian River, central Oklahoma, USA. *Chem. Geol.* **2009**, *265*, 455–467. [[CrossRef](#)]
13. Ingri, J.; Torssander, P.; Andersson, P.; Mörth, C.-M.; Kusakabe, M. Hydrogeochemistry of sulfur isotopes in the Kalix River catchment, northern Sweden. *Appl. Geochem.* **2015**, *12*, 483–496. [[CrossRef](#)]
14. Cortecchi, G.; Boschetti, T.; Dinelli, E.; Cabella, R. Sulphur isotopes, trace elements and mineral stability diagrams of waters from the abandoned Fe–Cu mines of Libiola and Vigonzano (Northern Apennines, Italy). *Water Air Soil Pollut.* **2008**, *192*, 85–103. [[CrossRef](#)]
15. Ma, Y.-H.; Su, C.-L.; Liu, W.-J.; Zhu, Y.-P.; Li, J.-X. Identification of sulfates sources in the groundwater system of Zaozhuang: Evidences from isotopic and hydrochemical characteristics. *Environ. Sci.* **2016**, *37*, 4690–4699.
16. Qiuxia, Z.; Jianwei, Z.; Fengxin, K.; Shanghua, L.; Dong, W.; Liming, Z.; Lei, Y. Hydrodynamic analysis and isotope tracing for probing into groundwater pollution of Zibo mining area. *Environ. Sci. Technol.* **2016**, *39*, 116–122.
17. Zhao, C.; Liang, Y.; Lu, H.; Tang, C.; Shen, H.; Wang, Z. SO_4^{2-} $\delta^{34}\text{S}$ Characteristics of Environmental Effects of Karst Water in Niangziguan Spring Group. *Carsologica Sin.* **2019**, *38*, 867–875.
18. *DZ/T 0064.49-2021*; Methods for Analysis of Groundwater Quality. Ministry of Natural Resources of the People's Republic of China: Beijing, China, 2021.
19. Huiming, B. Purifying barite for oxygen isotope measurement by dissolution and reprecipitation in a chelating solution. *Anal. Chem.* **2006**, *78*, 304–309.
20. Zhang, Q.; Wang, H.; Lu, C. Tracing sulfate origin and transformation in an area with multiple sources of pollution in northern China by using environmental isotopes and Bayesian isotope mixing model. *Environ. Pollut.* **2020**, *265*, 115105. [[CrossRef](#)]
21. *GB/T 14848-2017*; Standard for Groundwater Quality. Standardization Administration of China (SAC): Beijing, China, 2017.
22. Wang, Y.; Shi, L.; Qiu, M. Analysis of Chemical Characteristics of Mine Water based on Piper Trilinear Diagram. *Shandong Coal Sci. Technol.* **2019**, *4*, 145–147. [[CrossRef](#)]
23. Chidambaram, S.; Anandhan, P.; Prasanna, M.V.; Srinivasamoorthy, K.; Vasanthavignar, M. Major ion chemistry and identification of hydrogeochemical processes controlling groundwater in and around Neyveli Lignite Mines, Tamil Nadu, South India. *Arab. J. Geosci.* **2013**, *6*, 3451–3467. [[CrossRef](#)]
24. Tu, C.-L.; Yin, L.-H.; He, C.-Z.; Cun, D.-X.; Ma, Y.-Q.; Linghu, C.-W. Hydrochemical Composition Characteristics and Control Factors of Xiaohuangni River Basin in the upper Pearl River. *Environ. Sci.* **2022**, *43*, 1885–1897.
25. Gaillardet, J.; Dupré, B.; Louvat, P.; Allègre, C. Global silicate weathering and CO_2 consumption rates deduced from the chemistry of large rivers. *Chem. Geol.* **1999**, *159*, 30. [[CrossRef](#)]
26. Wang, Y.; Hu, Y.; Shen, J.; Qu, K.; Yin, N.; Yu, H.; Ma, G. Sulfur and Lead Isotope Composition and Tracing for Sources of Ore-forming Materials in Beiming River Iron Deposits, Southern Taihang Mountains. *Geoscience* **2011**, *25*, 846–852.
27. Xiao, H.; Liu, C.; Li, S. Geochemical Characteristics of Sulfur and Nitrogen Isotopic Compositions in Rains of Guiyang in Summer. *Geochimica* **2003**, *32*, 248–254.
28. Zhang, D.; Yang, J.; Huang, X.; Liu, S.; Zhang, Z. Sources of dissolved heavy metals in river water of the Yiluo River basin based on sulfur isotope of sulfate. *China Environ. Sci.* **2019**, *39*, 2549–2559.
29. Petelet-Giraud, E.; Klaver, G.; Negrel, P. Natural versus anthropogenic sources in the surface- and groundwater dissolved load of the Dommel river (Meuse basin): Constraints by boron and strontium isotopes and gadolinium anomaly. *J. Hydrol.* **2009**, *369*, 336–349. [[CrossRef](#)]
30. Hong, Y.; Zhang, H.; Zhu, Y.; Piao, H.; Jiang, H.; Liu, D. Characterization of sulfur isotope composition of atmospheric precipitation in China. *Prog. Nat. Sci.* **1994**, *4*, 741–745.
31. Li, X.; Gan, Y.; Zhou, A.; Liu, Y.; Wang, D. Hydrological controls on the sources of dissolved sulfate in the Heihe River, a large inland river in the arid Northwestern China, inferred from S and O isotopes. *Appl. Geochem.* **2013**, *35*, 99–109. [[CrossRef](#)]
32. Goldberg, T.; Poulton, S.W.; Strauss, H. Sulphur and oxygen isotope signatures of late Neoproterozoic to early Cambrian sulphate, Yangtze Platform, China: Diagenetic constraints and seawater evolution. *Precambrian Res.* **2005**, *137*, 223–241. [[CrossRef](#)]
33. Zhang, G.; Liu, C.Q.; Yang, Y.; Wu, P. Characterization of heavy metals and sulphur isotope in water and sediments of a mine-tailing area rich in carbonate. *Water Air Soil Pollut.* **2004**, *155*, 51–62. [[CrossRef](#)]
34. Kohl, I.; Bao, H. Triple-oxygen-isotope determination of molecular oxygen incorporation in sulfate produced during abiotic pyrite oxidation (pH = 2–11). *Geochim. Et. Cosmochim. Acta* **2011**, *75*, 1798. [[CrossRef](#)]
35. Zhang, H.; Wang, Z.; Pang, W.; Teng, Y.; Qi, H. Using sulfur and oxygen isotope to trace the source of sulphate in Baotuquan spring area of Jinan. *Geol. Surv. China* **2019**, *6*, 75–80.
36. Zhang, D.; Zhu, S.; Zhao, Z.; Li, H.; Yang, J.; Duan, H.; Guo, W.; Liu, Y. The Water-Sediment Regulation Scheme at Xiaolangdi Reservoir and Its Impact on Sulfur Cycling in the Yellow River Basin. *Earth Sci.* **2022**, *47*, 589–606.

Disclaimer/Publisher's Note: The statements, opinions and data contained in all publications are solely those of the individual author(s) and contributor(s) and not of MDPI and/or the editor(s). MDPI and/or the editor(s) disclaim responsibility for any injury to people or property resulting from any ideas, methods, instructions or products referred to in the content.